

# Diagnosis of Nerve Root Compromise of the Lumbar Spine: Evaluation of the Performance of Three-dimensional Isotropic T2-weighted Turbo Spin-Echo SPACE Sequence at 3T

Jinkyong Sung, MD<sup>1</sup>, Won-Hee Jee, MD<sup>1</sup>, Joon-Yong Jung, MD<sup>1</sup>, Jinhee Jang, MD<sup>1</sup>, Jin-Sung Kim, MD<sup>2</sup>, Young-Hoon Kim, MD<sup>3</sup>, Kee-Yong Ha, MD<sup>3</sup>

Departments of <sup>1</sup>Radiology, <sup>2</sup>Neurosurgery, and <sup>3</sup>Orthopedic Surgery, Seoul St. Mary's Hospital, College of Medicine, The Catholic University of Korea, Seoul 06591, Korea

**Objective:** To explore the performance of three-dimensional (3D) isotropic T2-weighted turbo spin-echo (TSE) sampling perfection with application optimized contrasts using different flip angle evolution (SPACE) sequence on a 3T system, for the evaluation of nerve root compromise by disc herniation or stenosis from central to extraforaminal location of the lumbar spine, when used alone or in combination with conventional two-dimensional (2D) TSE sequence.

**Materials and Methods:** Thirty-seven patients who had undergone 3T spine MRI including 2D and 3D sequences, and had subsequent spine surgery for nerve root compromise at a total of 39 nerve levels, were analyzed. A total of 78 nerve roots (48 symptomatic and 30 asymptomatic sites) were graded (0 to 3) using different MRI sets of 2D, 3D (axial plus sagittal), 3D (all planes), and combination of 2D and 3D sequences, with respect to the nerve root compromise caused by posterior disc herniations, lateral recess stenoses, neural foraminal stenoses, or extraforaminal disc herniations; grading was done independently by two readers. Diagnostic performance was compared between different imaging sets using the receiver operating characteristics (ROC) curve analysis.

**Results:** There were no statistically significant differences ( $p = 0.203$  to  $> 0.999$ ) in the ROC curve area between the imaging sets for both readers 1 and 2, except for combined 2D and 3D (0.843) vs. 2D (0.802) for reader 1 ( $p = 0.035$ ), and combined 2D and 3D (0.820) vs. 3D including all planes (0.765) for reader 2 ( $p = 0.049$ ).

**Conclusion:** The performance of 3D isotropic T2-weighted TSE sequence of the lumbar spine, whether axial plus sagittal images, or all planes of images, was not significantly different from that of 2D TSE sequences, for the evaluation of nerve root compromise of the lumbar spine. Combining 2D and 3D might possibly improve the diagnostic accuracy compared with either one.

**Keywords:** *Isotropic; Magnetic resonance imaging; Sampling perfection with application optimized contrasts using different flip angle evolution (SPACE); Lumbar spine; Nerve root compromise; Diagnosis*

Received December 16, 2015; accepted after revision August 12, 2016.

**Corresponding author:** Won-Hee Jee, MD, Department of Radiology, Seoul St. Mary's Hospital, College of Medicine, The Catholic University of Korea, 222 Banpo-daero, Seocho-gu, Seoul 06591, Korea.

• Tel: (822) 2258-6238 • Fax: (822) 599-6771  
• E-mail: whjee12@gmail.com

This is an Open Access article distributed under the terms of the Creative Commons Attribution Non-Commercial License (<http://creativecommons.org/licenses/by-nc/3.0>) which permits unrestricted non-commercial use, distribution, and reproduction in any medium, provided the original work is properly cited.

## INTRODUCTION

In recent years, three-dimensional (3D) isotropic magnetic resonance (MR) sequences have been increasingly used in musculoskeletal imaging due to its several intrinsic advantages as compared to two-dimensional (2D) fast spin-echo (FSE) sequences. The improved through-plane spatial resolution of 3D sequences reduces the partial-volume artifacts by obtaining thin continuous slices (1). Multiplanar reformation (MPR), which is necessary to evaluate anatomically complex musculoskeletal structures,

can be performed by post-processing (1). Not only the routine triplanar axis, but also dedicated oblique planes can be obtained without risk of misregistration, or an increase in imaging time (1). Moreover, the introduction of 3D isotropic FSE sequences enabled yielding similar tissue contrast characterization to conventional 2D FSE sequences, which was not possible on 3D gradient-echo sequences (2-4).

Many studies have shown that 3D isotropic sequences have similar image quality and diagnostic performance to conventional 2D sequences for the evaluation of internal derangements of the knee, shoulder, and ankle joints, when executed at 3T (4-8). In spine imaging, most of the studies using 3D isotropic sequences were feasibility studies reporting less artifacts and better delineation of small structures, or studies evaluating inter-method and inter-observer agreement (9-14). Recently, Lee et al. (15) compared 3D T2-weighted turbo spin-echo (TSE) and 2D T2-weighted TSE sequences of the lumbar spine, with surgical findings and symptoms. However, only nerve compression by posterior disc herniation correlated with the symptoms. We proposed that nerve compromise due to disc herniation or stenosis in every possible location from central to extraforaminal region should be considered for accurate symptomatic correlation. Thus, the purpose of this study was to explore the performance of 3D isotropic T2-weighted TSE sampling perfection with application optimized contrasts using different flip angle evolution (SPACE) sequence on a 3T system for the evaluation of nerve root compromise by disc herniation or stenosis from central to extraforaminal location of the lumbar spine, to be performed alone or in combination with conventional 2D TSE sequence.

## MATERIALS AND METHODS

### Patient Population

This study was approved by our Institutional Review Board and complied with Health Insurance Portability and Accountability Act (HIPAA) guidelines. The requirement to obtain informed consent was waived for this retrospective study. From March 2011 to February 2012, a 3D isotropic TSE sequence has been added to conventional 2D sequences in our hospital, when patients were suspected to have degenerative spinal disease or intervertebral disc herniation of the lumbar spine based on clinical examination, radiography, or CT. A total of 898 patients over 18 years of

age underwent lumbar spine MRI, including 3D isotropic TSE sequence at a 3T, to evaluate degenerative spinal disease or intervertebral disc herniation. Among them, we retrospectively identified 107 patients who had radicular leg pain, had subsequently undergone spine surgery for lumbar disc herniation or spinal stenosis, and who reported a decrease in symptoms after surgery. Seventy patients were excluded due to moderate to severe central spinal stenosis ( $n = 54$ ), adjacent two level involvement ( $n = 7$ ), and history or imaging evidence of previous spine surgery ( $n = 5$ ), infection ( $n = 1$ ), tumor ( $n = 1$ ), and fracture ( $n = 2$ ). Moderate and severe central spinal stenoses were defined as follows: moderate stenosis with some cauda equina aggregated; and severe stenosis with none of the cauda equina separated (16).

Thus, 37 patients with 39 nerve levels were included in the study: mean age, 52 years; age range, 20-74 years; 17 men (mean age, 46 years; age range, 20-71 years) and 20 women (mean age, 57 years; age range, 21-74 years). All patients complained of leg pain with a radicular distribution, and reported a decrease in or regression of symptoms after surgical treatment of the corresponding nerve level. The mean interval between MRI and surgery was 32 days (range, 0-117 days).

### MR Imaging Protocols

All 37 patients in the study group were imaged with a 3T MR unit (Magnetom Verio; Siemens, Erlangen, Germany) and a spine-array surface coil. Conventional 2D sequences consisted of a sagittal T1-weighted TSE sequence, and T2-weighted TSE sequences in the sagittal and axial planes. A 3D isotropic T2-weighted TSE sequence using SPACE with isotropic resolution, was acquired in the coronal plane. The imaging parameters of these sequences are summarized in Table 1. Driven-equilibrium radiofrequency pulse (Restore; Siemens Healthcare, Erlangen, Germany) was applied for 3D TSE SPACE. The source data acquired from 3D TSE SPACE sequences were subsequently reformatted into sagittal, axial, and oblique coronal images. Post-processing was performed by technologists at the imaging workstation, using commercially available software (Syngo MR; Siemens Healthcare). Reformation was performed with 0.6-mm slice thickness and without an interslice gap. On an average, reformation took about one minute.

### MR Imaging Analysis

Two radiologists (reader 1 and reader 2, with 17 and

### 3D SPACE of Lumbar Spine

3 years of experience in musculoskeletal radiology, respectively) who were blinded to the imaging reports, clinical history, and surgical findings, independently interpreted each set of conventional 2D and 3D isotropic TSE MR images to detect lumbar spinal nerve compromise of the operated level. First, sagittal and axial images from conventional 2D sequences were graded for nerve root compromise. Second, the sagittal- and axial-reformatted images from 3D isotropic T2-weighted TSE sequence were graded for the nerve root compromise. Third, sagittal-, axial-, coronal-, and oblique coronal images from 3D isotropic T2-weighted TSE sequence were graded for nerve root compromise. Fourth, combination of 2D (sagittal- and axial-images) and 3D isotropic (sagittal-, axial-, coronal-, and oblique coronal images) TSE sequences were graded for nerve root compromise. To prevent recall bias, there were

at least 6-week intervals between each review, and images were analyzed in a random order, different from that of previous reviews.

During each session, every MR imaging set was graded bilaterally for posterior or posterolateral disc herniation, lateral recess stenosis, neural foraminal stenosis, and extraforaminal disc herniation, which caused nerve root compromise.

Because of the lack of consensus regarding a grading system for lumbar disc herniation and spinal stenosis considering nerve root compromise (16-19), we modified the previous grading systems based on Pfirrmann's system (20), taking the surrounding structures into consideration. This modified grading system is summarized in Table 2.

**Table 1. MR Imaging Parameters**

Parameter	Isotropic 3D T2W-TSE (SPACE)	2D TSE (Conventional)		
		Sagittal T2	Axial T2	Sagittal T1
Repetition time (ms)	1500	4000	4000	845
Echo time (ms)	106	69	68	10
Echo train length	113	13	13	3
Intersection gap (mm)	0	0	0	0
Voxel size (mm)	0.6 x 0.6 x 0.6	0.5 x 1.1 x 3.0	0.3 x 0.6 x 4.0	0.5 x 1.1 x 3.0
Slice thickness (mm)	0.6	3	4	3
Field of view (mm)	270 x 270	256 x 280	153 x 153	256 x 280
Acquisition matrix	450 x 450	512 x 256	512 x 256	512 x 256
Bandwidth (Hz/pixel)	385	250	250	250
Acquisition time	6 min 54 sec	2 min 44 sec	4 min 56 sec	2 min 25 sec

MR = magnetic resonance, SPACE = sampling perfection with application optimized contrasts using different flip angle evolution, TSE = turbo spin-echo, T2W = T2-weighted, 2D = two-dimensional, 3D = three-dimensional

**Table 2. Grading of Nerve Root Compromise**

Grade	Posterior Disc Herniation	Lateral Recess Stenosis	Neural Foraminal Stenosis		Extraforaminal Disc Herniation	
	2D & 3D	2D & 3D	2D & 3D	3D	2D & 3D	3D
	Axial	Axial	Sagittal	Coronal	Axial	Coronal
0	No compromise	No compromise	No compromise	No compromise	No compromise	No compromise
1	Contact	Contact (one side)	Contact (< 180°)	Contact (2 sides, but not on the same craniocaudal line)	Contact	Contact (inferior portion of nerve)
2	Deviation	Contact (both sides, anterior and posterior) or medial deviation	Contact (180° ≤, ≤ 360°)	Contact (2 sides, on the same craniocaudal line)	Deviation (posterolateral)	Deviation (superolateral)
3	Compression	Compression	Compression	Compression	Compression (decreased thickness)	Compression (decreased thickness)

2D = two-dimensional, 3D = three-dimensional

### Reference Standard

A neurosurgeon, two orthopedic surgeons, and a physiatrist (each with more than 10 years of experience in their specialty) performed clinical examinations. Radicular leg pain was used as the reference standard. Level and lateral localization of the involved nerve were assessed on the basis of the patient's subjective symptoms and the clinician's physical examination which included a nerve tension test, recorded in the electronic medical records. Regression or a decrease in pain after operation was also assessed similarly. When physical examination was not sufficient to confirm radicular leg pain or localize the involved nerve, electromyography or preoperative block was also evaluated. On electromyography, the presence of positive sharp waves or fibrillation potentials were counted as positive, for both paraspinal and leg muscles (21).

### Statistical Analysis

Diagnostic performance of each reader was calculated using receiver operating characteristic (ROC) curve analyses. Area under the ROC curve (AUC) was obtained. To compare the diagnostic performances of 2D TSE sequences, 3D isotropic T2-weighted TSE sequences with and without coronal and oblique coronal images, and combination of 2D and 3D isotropic TSE sequences, pairwise comparisons of the ROC curves were performed. We used 95% confidence intervals to express the statistical precision of the results. Diagnostic sensitivity and specificity of each reader were calculated. Grade 2 and 3 were considered as a positive finding of nerve root compromise. Statistical differences in sensitivity and specificity among 2D conventional sequences, 3D isotropic T2-weighted TSE sequences with and without coronal and oblique coronal image, and combination of 2D and 3D isotropic TSE sequences, were assessed using McNemar statistics.

Interobserver agreement and intermodality agreement for detecting posterior or posterolateral disc herniation, lateral recess stenosis, neural foraminal stenosis, and extraforaminal disc herniation, were calculated using kappa coefficients. Kappa values were interpreted as follows: 0.00–0.20, slight agreement; 0.21–0.40, fair agreement; 0.41–0.60, moderate agreement; 0.61–0.80, substantial agreement; and 0.81–1.00, almost perfect agreement (22). For all tests,  $p < 0.05$  was considered indicative of a statistically significant difference. Given the exploratory nature of this study, we did not make an adjustment for multiple pairwise comparisons. All statistical analyses were

performed using commercial software (SPSS, version 19; SPSS Inc., Chicago, IL, USA), and MedCalc, version 11.3.0.0 (MedCalc, Mariakerke, Belgium).

## RESULTS

### Reference Standard

Of the 37 patients with 39 operated nerve levels, 4 cases had radicular leg pain correlating with L4 nerve involvement, 25 cases had L5 nerve involvement, and 10 cases had S1 nerve involvement. Unilateral symptoms were reported in 26 patients, and 11 patients had bilateral symptoms. Two patients with two level involvement had bilateral symptoms (unilateral symptom of each level). Regarding the lateral localization of pain, 17 cases were on the right side, 13 on the left side, and 9 on both sides. Thus, 48 symptomatic nerve roots and 30 asymptomatic nerve roots were evaluated.

### Diagnostic Performance

Diagnostic performances of 2D TSE and 3D TSE in the evaluation of overall nerve root compromise are shown in Table 3. AUCs (indicating diagnostic accuracy) of readers 1 and 2 for 2D T2-weighted TSE sequences and 3D isotropic T2-weighted TSE sequences with and without coronal and oblique coronal images, were not significantly different ( $p = 0.325$  to  $> 0.999$ ). AUCs of readers 1 and 2 for combination of 2D and 3D isotropic TSE sequences were higher than those of reader 1 for 2D ( $p = 0.035$ ) and reader 2 for 3D sequence (including all planes) ( $p = 0.049$ ), respectively. Of the 78 interpretations regarding bilateral nerves of the 39 levels, there were 12 false positive cases and 9 false negative cases. Both readers misinterpreted 8 false positive and 3 false negative cases on all sequences. At the second review of these cases, the diagnosis of the 11 cases that were misinterpreted on all sequences by both readers did not change, and we assumed these to be the cases showing poor association between clinical and imaging findings. Among the remaining 4 false positive cases, 1 case was reported as a grade 2 lateral recess stenosis on 3D sequence, by both readers (Fig. 1). Reader 1 and reader 2 misinterpreted 1 false positive case of lateral recess stenosis on 2D and 3D, respectively. Reader 2 misinterpreted 2 false positive cases of disc herniation on the 3D sequence. Among the remaining 6 false negative cases, both readers misinterpreted 2 cases of lateral recess stenosis (Fig. 2) and 1 case of disc herniation, on 2D sequences. Reader 1

### 3D SPACE of Lumbar Spine

and reader 2 misinterpreted 1 false negative case of disc herniation on 2D (reader 1) and all sequences (reader 2), and 1 extraforaminal disc herniation (Fig. 3) on 2D (reader 1) and 3D (axial and sagittal) (reader 2), respectively. Reader 2 missed 1 lateral recess stenosis on all sequences. Example of posterior disc herniation and neural foraminal stenosis are shown in Figures 4, 5.

#### Interobserver Agreement

Interobserver agreement was almost perfect for 2D and 3D sequences in the evaluation of all causes of nerve root compromise, including posterior or posterolateral

disc herniation, lateral recess stenosis, neural foraminal stenosis, and extraforaminal disc herniation (Table 4). Kappa ranged from 0.88 (lateral recess stenosis on 2D T2-weighted TSE sequences) to 0.97 (posterior or posterolateral disc herniation on 2D T2-weighted TSE sequences and extraforaminal disc herniation on 3D isotropic T2-weighted TSE with coronal or oblique coronal images).

#### DISCUSSION

In this study, the diagnostic performance of 3D isotropic T2-weighted TSE sequence of the lumbar spine was not

**Table 3. Diagnostic Performance of 2D TSE and 3D TSE and AUCs for Evaluation of Nerve Root Compromise**

	Sensitivity (%)	Specificity (%)	AUC
<b>2D TSE</b>			
Reader 1	83.3 (40/48)	63.3 (19/30)	0.802 (0.697, 0.884)
Reader 2	81.3 (39/48)	66.7 (20/30)	0.797 (0.690, 0.879)
<b>3D TSE (Ax and Sag)</b>			
Reader 1	93.8 (45/48)	63.3 (19/30)	0.820 (0.716, 0.898)
Reader 2	87.5 (42/48)	53.3 (16/30)	0.764 (0.654, 0.853)
<b>3D TSE (Ax, Sag, Cor, and Obl Cor)</b>			
Reader 1	93.8 (45/48)	63.3 (19/30)	0.820 (0.716, 0.898)
Reader 2	89.6 (43/48)	53.3 (16/30)	0.765 (0.655, 0.853)
<b>Combination of 2D and 3D</b>			
Reader 1	93.8 (45/48)	63.3 (19/30)	0.843 (0.743, 0.916)
Reader 2	89.6 (43/48)	63.3 (19/30)	0.820 (0.717, 0.898)
<i>p</i> value			
<b>2D TSE vs. 3D TSE (Ax and Sag)</b>			
Reader 1	0.063	> 0.999	0.540
Reader 2	0.250	0.125	0.325
<b>2D TSE vs. 3D TSE (Ax, Sag, Cor, and Obl Cor)</b>			
Reader 1	0.063	> 0.999	0.540
Reader 2	0.125	0.125	0.341
<b>3D TSE (Ax and Sag) vs. 3D TSE (Ax, Sag, Cor, and Obl Cor)</b>			
Reader 1	> 0.999	> 0.999	> 0.999
Reader 2	> 0.999	> 0.999	0.927
<b>2D TSE vs. combination of 2D and 3D</b>			
Reader 1	0.125	> 0.999	0.035
Reader 2	0.125	> 0.999	0.203
<b>3D TSE (Ax and Sag) vs. combination of 2D and 3D</b>			
Reader 1	> 0.999	> 0.999	0.248
Reader 2	> 0.999	0.125	0.050
<b>3D TSE (Ax, Sag, Cor, and Obl Cor) vs. combination of 2D and 3D</b>			
Reader 1	> 0.999	> 0.999	0.248
Reader 2	> 0.999	0.250	0.049

Data in brackets are 95% confidence intervals. Combination of 2D and 3D is combination of 2D TSE (axial and sagittal images) and 3D TSE (axial [Ax], sagittal [Sag], coronal [Cor], and oblique coronal [Obl Cor] images) sequences. For sensitivity, specificity, and accuracy of MR sequences, data in parentheses are raw data. AUC = area under the receiver operating characteristic curve, TSE = turbo spin-echo, 2D = two-dimensional, 3D = three-dimensional

significantly different from that of conventional 2D TSE sequences in the evaluation of nerve root compromise. The combination of 2D and 3D might improve the diagnostic accuracy of readers. In addition, 3D isotropic sequence showed excellent interobserver agreement.

In our study, two of the three false negative cases on

2D sequences by both readers were lateral recess stenosis. Because the narrowest portion of the lateral recess is its cephalic portion at the superior border of the pedicle, it is important to evaluate the most cephalic portion where the nerve root is commonly compressed (23). However, when using axial images from 2D TSE sequences of 4-mm

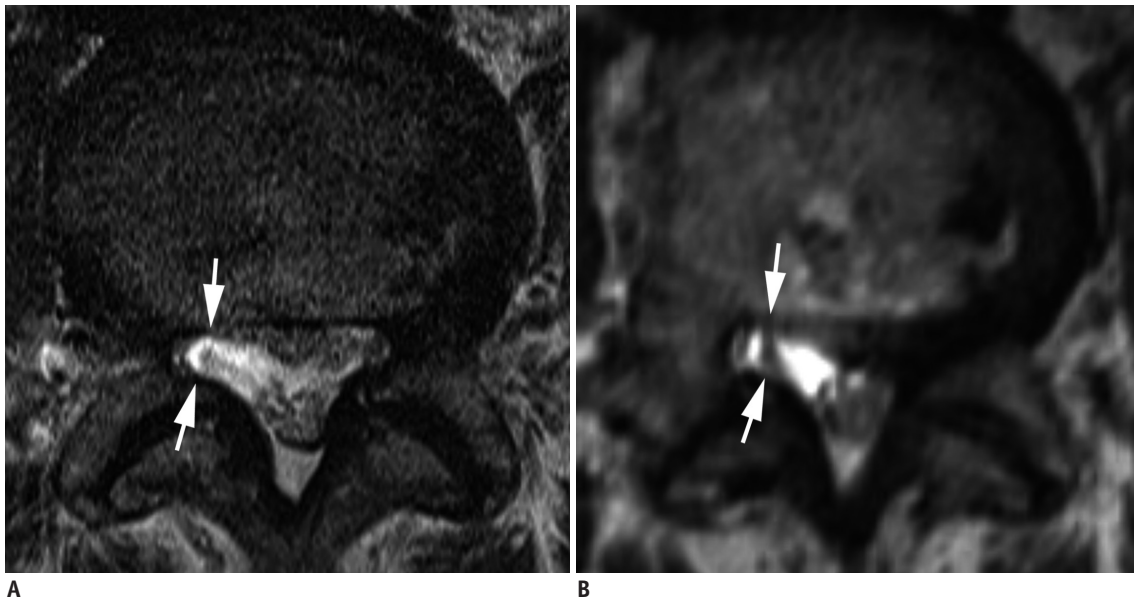


**Fig. 1. Axial MR images of 74-year-old woman with left radicular leg pain along L5 dermatome.**

Axial 2D T2-weighted TSE image (A) shows non-compromised right L5 nerve root (arrows) without contact with adjacent structures. However, both readers scored this finding on axial 3D isotropic T2-weighted TSE image (B) as grade 2 lateral recess stenosis (arrows) because of image blurring. MR = magnetic resonance, TSE = turbo spin-echo, 2D = two-dimensional, 3D = three-dimensional

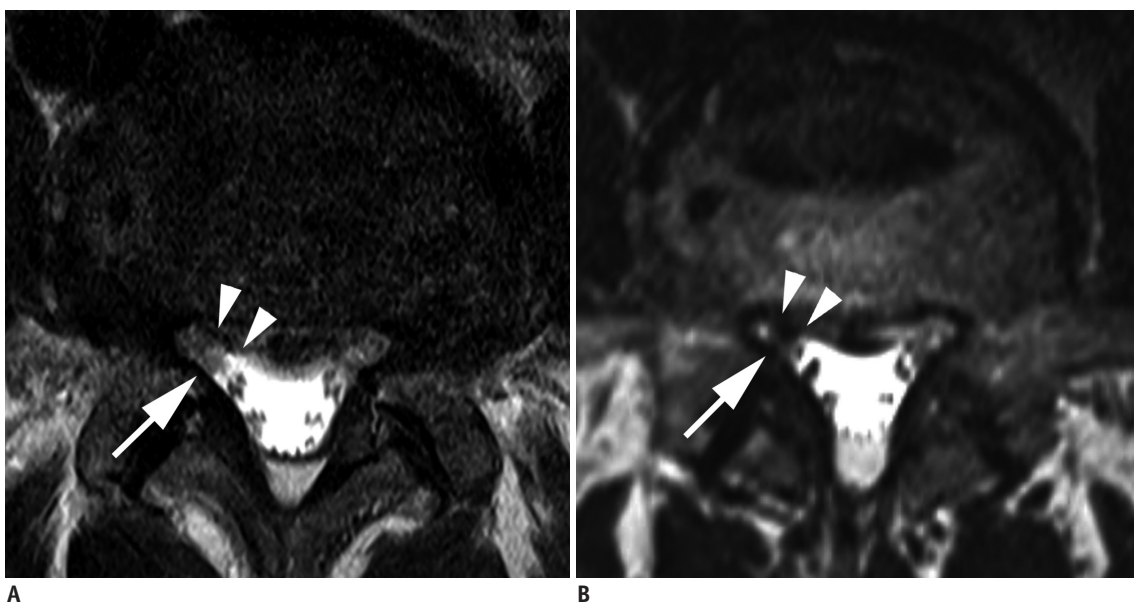


**Fig. 2. Axial MR images in 61-year-old man with right radicular leg pain along L5 dermatome.**

Axial 2D T2-weighted TSE image (A) shows herniated disc (arrowheads) and non-compromised right L5 nerve root (arrow). However, both readers correctly interpreted compressed right L5 nerve root (arrow) by herniated disc (arrowheads) at right lateral recess stenosis on axial 3D isotropic T2-weighted TSE image (B). There were no other findings compromising right L5 nerve root. MR = magnetic resonance, TSE = turbo spin-echo, 2D = two-dimensional, 3D = three-dimensional

thickness, partial volume artifacts are inevitable, and the image may be insufficient to evaluate the lateral recess at the exact superior border level of the pedicle. Disc material, ligamentum flavum thickening, or facet hypertrophy at the intervertebral disc level can appear as if they are at the lateral recess level, and vice versa. Because the improved through-plane spatial resolution of 3D isotropic T2-weighted TSE sequence reduced partial volume artifacts by obtaining thin contiguous slices (0.6 mm thickness in our study)

and reformatting with thin slices (0.6 mm thickness in our study) without an interslice gap, we were able to detect lateral recess stenoses on 3D images that were missed on 2D TSE sequences.

Reduced partial volume artifacts also influenced the nerve root evaluation of the extraforaminal zone. The nerve exiting the neural foramen descends obliquely downward and outward at the extraforaminal zone. Because of its oblique course, when the nerve is very close to the

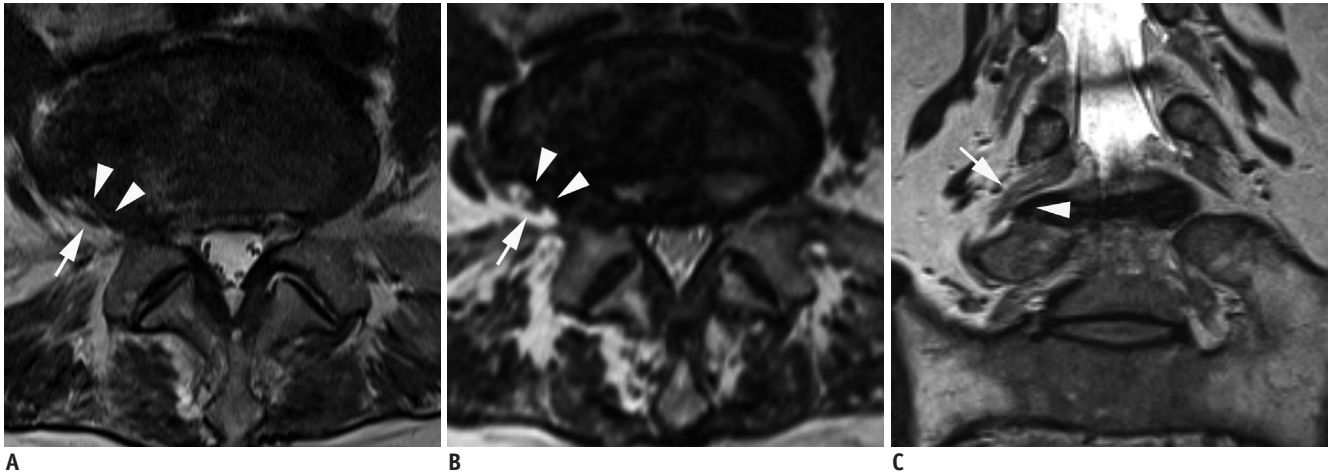


**Fig. 3.** MR images in 70-year-old woman with right radicular leg pain along L5 dermatome.

Axial 2D T2-weighted image (A) shows extraforaminal disc herniation and suspiciously deviated right L5 nerve root. Axial 3D T2-weighted image (B) at same level shows suspiciously deviated right L5 nerve root having contact with herniated extraforaminal disc. Reader 1 missed this lesion on 2D images, and reader 2 missed this lesion on both 2D and 3D axial images. However, both readers correctly interpreted this lesion on 3D sequence with coronal and oblique coronal images. Superolaterally deviated right L5 nerve root is more definitely delineated on coronal 3D isotropic T2-weighted TSE image (C). There were no other findings compromising right L5 nerve root. MR = magnetic resonance, TSE = turbo spin-echo, 2D = two-dimensional, 3D = three-dimensional

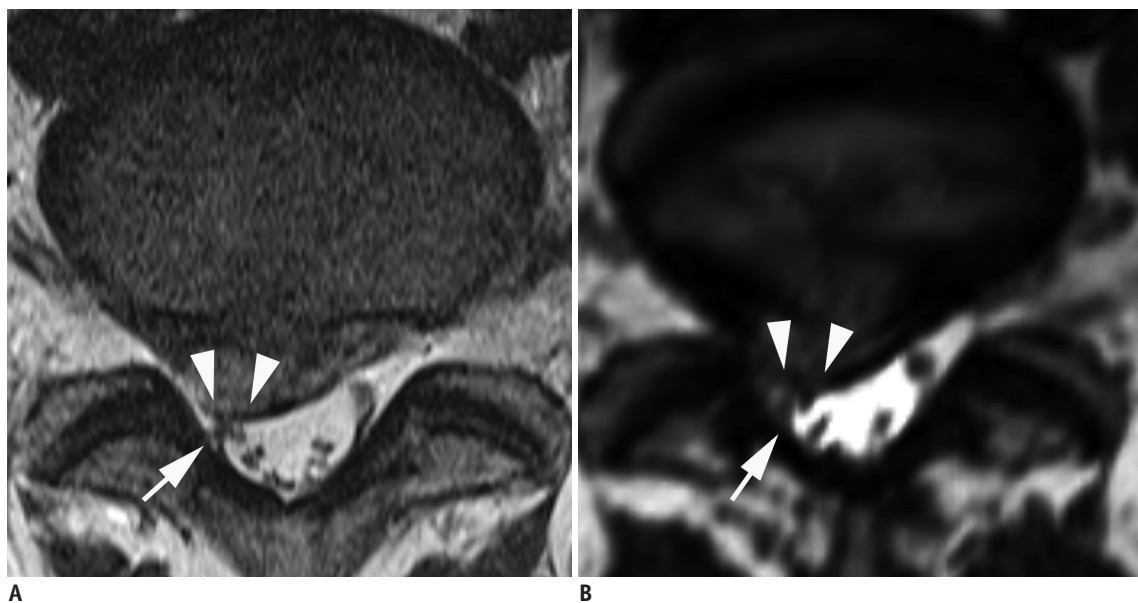


**Fig. 4.** Axial MR images in 23-year-old woman with right radicular leg pain along S1 dermatome.

Axial 2D T2-weighted TSE image (A) and axial 3D isotropic T2-weighted TSE image (B) show deviated right S1 nerve root (arrows) by right central disc protrusion (arrowheads). MR = magnetic resonance, TSE = turbo spin-echo, 2D = two-dimensional, 3D = three-dimensional

herniated extraforaminal disc, nerve root just above or below the disc appears as if it is at the same plane with the disc on 2D sequence due to partial volume artifact (6, 15). Thus, the actual contact can be missed, or the preserved fat between disc and nerve root can be obscured. Because the extent of sagittal imaging plane of conventional 2D TSE sequence is limited in the evaluation of extraforaminal zone, obtaining coronal and oblique coronal images with larger field of view in the 3D isotropic T2-weighted TSE sequence enabled delineation of the extraforaminal nerve root and adjacent structures in the longitudinal plane.

Although images of 3D isotropic TSE sequence with a thinner slice thickness provides greater through-plane resolution than 2D TSE sequences, inferior in-plane resolution and image blurring are well known weakness of 3D isotropic TSE sequence (4, 6, 8, 24). In spinal imaging, these factors can hinder discriminating the small

nerve roots and adjacent structures that can cause nerve root compromise. In this study, determining whether the nerve was in contact with adjacent structure was sometimes difficult to decipher. Nevertheless, because both grades 0 and 1 were categorized as negative findings for symptomatic correlation, only 1 false positive case was observed in 3D isotropic TSE sequence by both readers.

The acquisition time of 3D isotropic T2-weighted TSE sequence was 6 minutes 54 seconds in this study, which was about 3 minutes shorter than the total acquisition time of 2D TSE sequences (10 minutes 5 seconds), and about 1 minute shorter than that of 2D T2-weighted TSE sequences (7 minutes 40 seconds). Additionally, we could also get coronal and oblique coronal images by postprocessing, and there were no cases showing motion artifact affecting image analysis. Although in this study, additional coronal images changed diagnosis of only one false negative case to correct

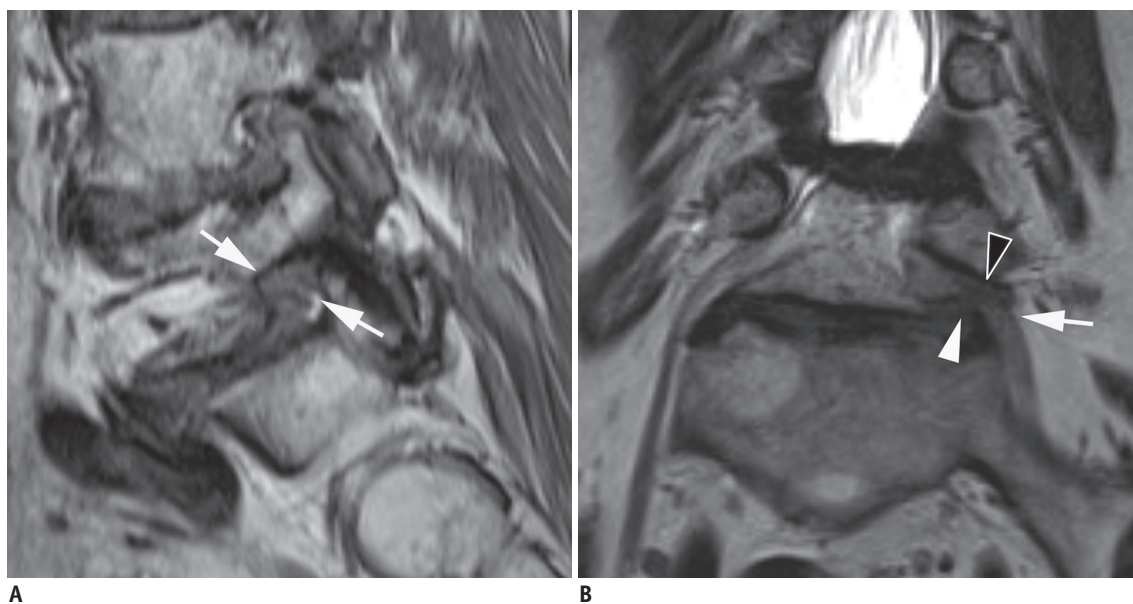


**Fig. 5. MR images in 74-year-old woman with left radicular leg pain along L5 dermatome.**

**A.** Sagittal 2D T1-weighted TSE image shows compressed L5 nerve root of left L5-S1 neural foramen (arrows). **B.** Compressed nerve root (arrow) by extruded foraminal disc (white arrowhead) and facet hypertrophy (black arrowhead) is also well visible on coronal 3D isotropic T2-weighted TSE image. Both readers correctly interpreted grade 3 neural foraminal stenosis. MR = magnetic resonance, TSE = turbo spin-echo, 2D = two-dimensional, 3D = three-dimensional

**Table 4. Interobserver Agreement for Evaluation of Nerve Compromise**

	Interobserver Agreement (Kappa)		
	2D TSE	3D TSE (Ax and Sag)	3D TSE (Ax, Sag, Cor, and Obl Cor)
Overall nerve compromise	0.93 (0.87, 0.99)	0.88 (0.81, 0.96)	0.91 (0.83, 0.98)
Posterior or posterolateral disc herniation	0.97 (0.94, 1.00)	0.94 (0.89, 1.00)	0.93 (0.88, 0.99)
Lateral recess stenosis	0.88 (0.79, 0.97)	0.92 (0.87, 0.98)	0.92 (0.86, 0.98)
Neural foraminal stenosis	0.94 (0.88, 1.00)	0.94 (0.88, 1.00)	0.90 (0.82, 0.97)
Extraforaminal disc herniation	0.95 (0.89, 1.00)	0.91 (0.85, 0.98)	0.97 (0.92, 1.00)

Data in brackets are 95% confidence interval. All *p* values are < 0.001. Ax = axial, Cor = coronal, Obl Cor = oblique coronal, Sag = sagittal, TSE = turbo spin-echo, 2D = two-dimensional, 3D = three-dimensional

## 3D SPACE of Lumbar Spine

interpretation in reader 2, despite changes of the grades in several cases, MPR capability of 3D isotropic TSE sequence will be especially useful in patients with severe scoliosis or kyphosis, which consumes more time to obtain oblique axial and oblique sagittal images at different planes.

Unlike previous studies that evaluated the spine using sagittal 3D sequence (9, 10, 15), we obtained coronal 3D isotropic T2-weighted TSE images. Initially, we performed sagittal 3D isotropic T2-weighted TSE sequence for lumbar spine evaluation. However, because of the large transverse diameter of the body, aliasing artifacts were present despite a relatively long scan time (about 9 minutes). These artifacts mainly affected the evaluation of extraforaminal lesions. After obtaining 3D isotropic T2-weighted TSE image on coronal axis, aliasing artifacts did not occur, and the scan time was reduced because of the smaller anteroposterior diameter.

Lateral localization of radicular leg pain was used as a standard of reference. Because of the retrospective design of the study, detailed correlation with surgical findings for all probable causes of nerve root compromise according to anatomic location was not possible. Although anatomic changes are not highly correlated with clinical symptoms in lumbar spinal stenosis, the nerve root compromise by posterior and extraforaminal disc herniation, and lateral recess and foraminal stenosis are known to predict radicular symptoms relatively well, with an increase in sensitivity following an increase in severity (25-30). Moreover, as we selected only operated levels of symptomatic patients who reported decrease in pain after surgery, we were able to infer that nerve root compromise at the operated level was responsible for the patient's radicular symptoms. For symptomatic correlation, we excluded moderate to severe central canal stenosis, which is more likely to cause neurogenic claudication or referred pain from degenerative facet joints or ligaments (25, 29). Although referred pain and neurogenic claudication have different clinical features from radicular pain and can be differentiated by some provocation tests, these can be confused in clinical practice and can coexist in severe cases. Exclusion of moderate to severe central spinal stenosis might contribute to the high interobserver agreement in this study due to exclusion of more confusing cases.

Despite the frequency and importance of imaging studies in the evaluation of lumbar spinal stenosis and disc herniation, various quantitative and qualitative diagnostic criteria and grading systems exist, and there are no widely

accepted grading systems. Qualitative criteria have strength in its consideration of anatomic structures causing stenosis, and are more widely used among experts in musculoskeletal radiology (16-20, 31). However they are not always clear, and are often applied in combination or in a modified way (25, 31, 32). Because the presence of nerve root compromise, especially in severe cases, is known to be an important predictor of radicular leg pain, we graded disc herniation and spinal stenoses according to the degree of nerve compromise. Grades 2 and 3 are considered to be positive findings with regards to correlating with the symptoms (20, 26, 28).

This study had several limitations. First, there is the possibility of selection bias because of the retrospective design of the study, and inclusion of patients who had symptoms and underwent surgery. This might have increased diagnostic performance in our study. Second, the reviewers who evaluated MR images were aware that all patients had undergone surgery and they were evaluating operated levels, although they did not know detailed surgical findings or surgical procedure. This could have introduced reader bias, which might have led to the high diagnostic performance. Third, even though all patients underwent an operation, detailed correlation with surgical findings for all possible causes of nerve compromise according to anatomic location was not possible in this retrospective study. Despite the fact that clinical symptoms are not always highly correlated with imaging findings, and the possibility of chemical radiculitis that can also cause radiculopathy, we reasoned that the radicular leg pain of patients who reported a decrease in pain after surgery of the corresponding level would be sufficient as a reference standard. Fourth, because possible causes of nerve compromise at four different anatomic locations contributed to one symptom, coexisting nerve root compromise findings at different locations could not be correlated with the standard reference independently. Fifth, the study population was relatively small, despite the high incidence of degenerative spine disease. For symptomatic correlation, stricter inclusion criteria should be applied.

In conclusion, the performance of 3D isotropic T2-weighted TSE sequence of the lumbar spine, whether axial plus sagittal images or all planes of images, was not significantly different from that of 2D TSE sequences in the evaluation of nerve root compromise of the lumbar spine. Combining 2D and 3D might possibly improve diagnostic accuracy, as compared with either one.

## REFERENCES

1. Naraghi A, White LM. Three-dimensional MRI of the musculoskeletal system. *AJR Am J Roentgenol* 2012;199:W283-W293
2. Lichy MP, Wietek BM, Mugler JP 3rd, Horger W, Menzel MI, Anastasiadis A, et al. Magnetic resonance imaging of the body trunk using a single-slab, 3-dimensional, T2-weighted turbo-spin-echo sequence with high sampling efficiency (SPACE) for high spatial resolution imaging: initial clinical experiences. *Invest Radiol* 2005;40:754-760
3. Gold GE, Busse RF, Beehler C, Han E, Brau AC, Beatty PJ, et al. Isotropic MRI of the knee with 3D fast spin-echo extended echo-train acquisition (XETA): initial experience. *AJR Am J Roentgenol* 2007;188:1287-1293
4. Stevens KJ, Busse RF, Han E, Brau AC, Beatty PJ, Beaulieu CF, et al. Ankle: isotropic MR imaging with 3D-FSE-cube--initial experience in healthy volunteers. *Radiology* 2008;249:1026-1033
5. Jung JY, Yoon YC, Kwon JW, Ahn JH, Choe BK. Diagnosis of internal derangement of the knee at 3.0-T MR imaging: 3D isotropic intermediate-weighted versus 2D sequences. *Radiology* 2009;253:780-787
6. Kijowski R, Davis KW, Woods MA, Lindstrom MJ, De Smet AA, Gold GE, et al. Knee joint: comprehensive assessment with 3D isotropic resolution fast spin-echo MR imaging--diagnostic performance compared with that of conventional MR imaging at 3.0 T. *Radiology* 2009;252:486-495
7. Choo HJ, Lee SJ, Kim OH, Seo SS, Kim JH. Comparison of three-dimensional isotropic T1-weighted fast spin-echo MR arthrography with two-dimensional MR arthrography of the shoulder. *Radiology* 2012;262:921-931
8. Jung JY, Jee WH, Park MY, Lee SY, Kim YS. SLAP tears: diagnosis using 3-T shoulder MR arthrography with the 3D isotropic turbo spin-echo space sequence versus conventional 2D sequences. *Eur Radiol* 2013;23:487-495
9. Kwon JW, Yoon YC, Choi SH. Three-dimensional isotropic T2-weighted cervical MRI at 3T: comparison with two-dimensional T2-weighted sequences. *Clin Radiol* 2012;67:106-113
10. Meindl T, Wirth S, Weckbach S, Dietrich O, Reiser M, Schoenberg SO. Magnetic resonance imaging of the cervical spine: comparison of 2D T2-weighted turbo spin echo, 2D T2\*weighted gradient-recalled echo and 3D T2-weighted variable flip-angle turbo spin echo sequences. *Eur Radiol* 2009;19:713-721
11. Rodegerdts EA, Boss A, Riemarzik K, Lichy M, Schick F, Claussen CD, et al. 3D imaging of the whole spine at 3T compared to 1.5T: initial experiences. *Acta Radiol* 2006;47:488-493
12. Tins B, Cassar-Pullicino V, Haddaway M, Nachtrab U. Three-dimensional sampling perfection with application-optimised contrasts using a different flip angle evolutions sequence for routine imaging of the spine: preliminary experience. *Br J Radiol* 2012;85:e480-e489
13. Blizzard DJ, Haims AH, Lischuk AW, Arunakul R, Hustedt JW, Grauer JN. 3D-FSE isotropic MRI of the lumbar spine: novel application of an existing technology. *J Spinal Disord Tech* 2015;28:152-157
14. Fu MC, Buerba RA, Neway WE 3rd, Brown JE, Trivedi M, Lischuk AW, et al. Three-dimensional isotropic MRI of the cervical spine: a diagnostic comparison with conventional MRI. *Clin Spine Surg* 2016;29:66-71
15. Lee S, Jee WH, Jung JY, Lee SY, Ryu KS, Ha KY. MRI of the lumbar spine: comparison of 3D isotropic turbo spin-echo SPACE sequence versus conventional 2D sequences at 3.0 T. *Acta Radiol* 2015;56:174-181
16. Lee GY, Lee JW, Choi HS, Oh KJ, Kang HS. A new grading system of lumbar central canal stenosis on MRI: an easy and reliable method. *Skeletal Radiol* 2011;40:1033-1039
17. Schizas C, Theumann N, Burn A, Tansey R, Wardlaw D, Smith FW, et al. Qualitative grading of severity of lumbar spinal stenosis based on the morphology of the dural sac on magnetic resonance images. *Spine (Phila Pa 1976)* 2010;35:1919-1924
18. Lee S, Lee JW, Yeom JS, Kim KJ, Kim HJ, Chung SK, et al. A practical MRI grading system for lumbar foraminal stenosis. *AJR Am J Roentgenol* 2010;194:1095-1098
19. Bartynski WS, Lin L. Lumbar root compression in the lateral recess: MR imaging, conventional myelography, and CT myelography comparison with surgical confirmation. *AJNR Am J Neuroradiol* 2003;24:348-360
20. Pfirmann CW, Dora C, Schmid MR, Zanetti M, Hodler J, Boos N. MR image-based grading of lumbar nerve root compromise due to disk herniation: reliability study with surgical correlation. *Radiology* 2004;230:583-588
21. Tong HC, Haig AJ, Yamakawa KS, Miner JA. Specificity of needle electromyography for lumbar radiculopathy and plexopathy in 55- to 79-year-old asymptomatic subjects. *Am J Phys Med Rehabil* 2006;85:908-912; quiz 913-915, 934
22. Landis JR, Koch GG. An application of hierarchical kappa-type statistics in the assessment of majority agreement among multiple observers. *Biometrics* 1977;33:363-374
23. Mikhael MA, Ciric I, Tarkington JA, Vick NA. Neuroradiological evaluation of lateral recess syndrome. *Radiology* 1981;140:97-107
24. Busse RF, Hariharan H, Vu A, Brittain JH. Fast spin echo sequences with very long echo trains: design of variable refocusing flip angle schedules and generation of clinical T2 contrast. *Magn Reson Med* 2006;55:1030-1037
25. Genevay S, Atlas SJ. Lumbar spinal stenosis. *Best Pract Res Clin Rheumatol* 2010;24:253-265
26. Beattie PF, Meyers SP, Stratford P, Millard RW, Hollenberg GM. Associations between patient report of symptoms and anatomic impairment visible on lumbar magnetic resonance imaging. *Spine (Phila Pa 1976)* 2000;25:819-828
27. Weishaupt D, Zanetti M, Hodler J, Boos N. MR imaging of the lumbar spine: prevalence of intervertebral disk extrusion and sequestration, nerve root compression, end plate abnormalities, and osteoarthritis of the facet joints in

### 3D SPACE of Lumber Spine

- asymptomatic volunteers. *Radiology* 1998;209:661-666
28. Modic MT, Obuchowski NA, Ross JS, Brant-Zawadzki MN, Grooff PN, Mazanec DJ, et al. Acute low back pain and radiculopathy: MR imaging findings and their prognostic role and effect on outcome. *Radiology* 2005;237:597-604
  29. Siebert E, Prüss H, Klingebiel R, Failli V, Einhäupl KM, Schwab JM. Lumbar spinal stenosis: syndrome, diagnostics and treatment. *Nat Rev Neurol* 2009;5:392-403
  30. Lee IS, Kim HJ, Lee JS, Moon TY, Jeon UB. Extraforaminal with or without foraminal disk herniation: reliable MRI findings. *AJR Am J Roentgenol* 2009;192:1392-1396
  31. Mamisch N, Brumann M, Hodler J, Held U, Brunner F, Steurer J; Lumbar Spinal Stenosis Outcome Study Working Group Zurich. Radiologic criteria for the diagnosis of spinal stenosis: results of a Delphi survey. *Radiology* 2012;264:174-179
  32. Andreisek G, Hodler J, Steurer J. Uncertainties in the diagnosis of lumbar spinal stenosis. *Radiology* 2011;261:681-684